

Theoretical spectral analysis of FEL radiation from multi-harmonic undulators. Corrigendum

K. Zhukovsky*

Department of Theoretical Physics, Faculty of Physics, M. V. Lomonosov Moscow State University, Moscow 119991, Russian Federation. *Correspondence e-mail: zhukovsk@physics.msu.ru

Received 4 December 2020

Accepted 13 January 2021

Edited by M. Yamamoto, RIKEN Spring-8 Center, Japan

Keywords: undulator; field harmonics; radiation harmonics; free-electron laser.

A correction to an equation in the paper by Zhukovsky [(2020). *J. Synchrotron Rad.* **27**, 1648–1661] is made and, following from this, values of some Bessel coefficients and some harmonic intensities from an elliptic undulator with the third field harmonic.

The author would like to correct a misprint in formula (3) of Zhukovsky (2020) and communicate the change of the numerical values in equations (23), (24) and in Fig. 9.

The argument of the generalized Bessel function (3) in Zhukovsky (2020) for the magnetic field

$$\mathbf{H} = H_0 [\sin(k_\lambda z) + d \sin(pk_\lambda z), d_1 \sin(hk_\lambda z) + d_2 \cos(lk_\lambda z), 0],$$

$$k_\lambda = 2\pi/\lambda_{u,x}, \quad d, d_1, d_2 \in \text{real}, \quad h, l, p \in \text{integers}, \quad (1)$$

was erroneously written in equation (3) of Zhukovsky (2020) as a cosine instead of an exponential; formula (3) should correctly read as follows,

$$J_n^m(\xi_i) = \int_0^{2\pi} \frac{d\alpha}{2\pi} \exp \left(i \left\{ n\alpha + \xi_1 \sin(h\alpha) + \xi_2 \cos(l\alpha) \right. \right.$$

$$+ \xi_3 \sin \alpha + \xi_4 \sin(2\alpha) + \xi_5 \sin(2h\alpha)$$

$$+ \xi_6 \sin(2l\alpha) + \xi_7 \cos[(l+h)\alpha]$$

$$+ \xi_8 \cos[(l-h)\alpha] + \xi_0 \sin(p\alpha)$$

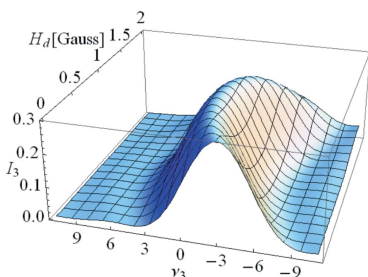
$$+ \xi_9 \sin[(p+1)\alpha] + \xi_{10} \sin[(p-1)\alpha]$$

$$\left. \left. + \xi_{11} \sin(2p\alpha) \right\} \right). \quad (3)$$

The undulator radiation (UR) harmonic powers in the undulator with $N = 30$ periods, $k = 2.216$ and period $\lambda_u = 2.3$ cm, and the beam with energy spread $\sigma_e = 0.1\%$, are shown here in the revised versions of Figures 9(a) and 9(b), which replace the respective figures in the original paper. The ratio between the harmonic intensity of the undulator and the magnetic field (21) [see Zhukovsky (2020)] has somewhat changed, but, for the studied undulator field (22) in Zhukovsky (2020),

$$\mathbf{H} = H_0 [\sin(k_\lambda z), 0.25 \cos(k_\lambda z) + \sin(3k_\lambda z), 0],$$

the third UR harmonic remains strong in both polarizations and the change of the Bessel coefficients for the third harmonic, $f_{n=3}$, is minor as compared with their values in Zhukovsky (2020). New values, reported below, substitute those in formulae (23) and (24) of Zhukovsky (2020),



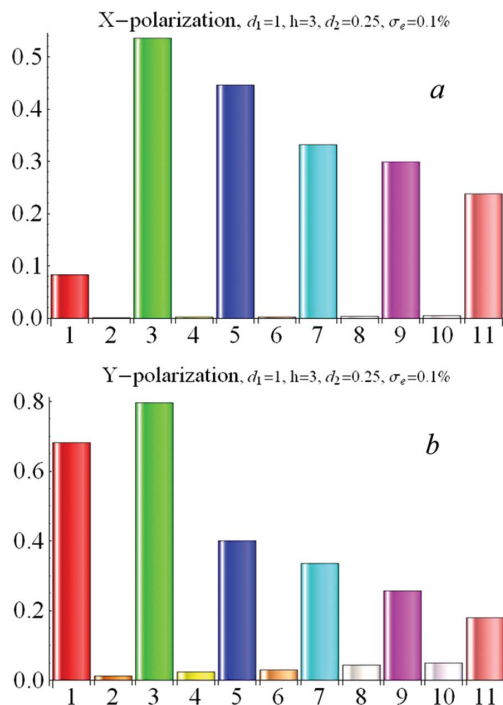


Figure 9
 (a) x-polarization and (b) y-polarization of the on-axis UR harmonics intensity (in relative units) for the elliptic undulator with period $\lambda_u = 2.3$ cm, $k = 2.21622$, $h = 3$, $d_1 = 1$, $d_2 = +0.25$, $l = 1$, $\sigma_e = 10^{-3}$, $N = 30$.

$$f_{x;n=1\dots9} = \{0.290, 0.007, 0.256, 0.010, 0.151, 0.009, 0.101, 0.009, 0.081\}, \quad (23)$$

$$f_{y;n=1\dots9} = \{0.830, 0.056, 0.313, 0.042, 0.143, 0.033, 0.102, 0.033, 0.075\}. \quad (24)$$

The changes of the numerical values in (26), (27), (29), (30) are minor and we omit them for brevity. The harmonic intensities of the UR spectrum, obtained with formula (3) for the undulator in Zhukovsky (2020), are now revised and reported in the revised Figures 9(a) and 9(b) for x- and y-polarizations, respectively. We consider [see also Zhukovsky (2020)] an undulator with period $\lambda_u = 2.3$ cm, $k = 2.216$, magnetic field given by (22), electron beam relativistic parameter $\gamma = 12.72$, emittances $\epsilon_x = 1.5$ mm mrad and $\epsilon_y = 0.35$ mm mrad, Twiss parameters $\beta_x = 43.66$ cm and $\beta_y = 28.75$ cm, beam sections $\sigma_x = 809$ μ m and $\sigma_y = 317$ μ m, divergences $\theta_x = 4.5$ mrad and $\theta_y = 1.6$ mrad and electron energy spread $\sigma_e = 0.1\%$. The corrections have not affected other calculations, results and conclusions in Zhukovsky (2020). The author apologizes for the inconvenience.

References

Zhukovsky, K. (2020). *J. Synchrotron Rad.* **27**, 1648–1661.

Theoretical spectral analysis of FEL radiation from multi-harmonic undulators

K. Zhukovsky*

Department of Theoretical Physics, Faculty of Physics, M. V. Lomonosov Moscow State University, Moscow 119991, Russian Federation. *Correspondence e-mail: zhukovsk@physics.msu.ru

Received 28 May 2020

Accepted 3 September 2020

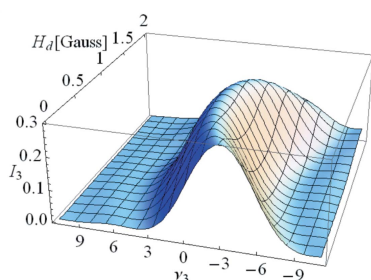
Edited by M. Yamamoto, RIKEN Spring-8 Center, Japan

Keywords: undulator; field harmonics; radiation harmonics; free-electron laser.

A theoretical study of the spontaneous and stimulated undulator radiation (UR) from electrons in undulators with multiple periods in both transversal directions is presented. Exact expressions are derived for the UR intensities in terms of the generalized Bessel and Airy functions, accounting for undulator field harmonics of arbitrary strength and for real parameters of the beams and installations. Theoretical results are verified with numerical and experimental data for SWISS-XFEL, PAL-XFEL, LEUTL, LCLS *etc.* The spectrum, UR line shape and width, and the harmonic evolution along the undulators are analyzed and compared with the available data for these experiments. Moreover, the effect of the field harmonics is elucidated. It is demonstrated that the third field harmonic can cause distinct odd UR harmonics. The asymmetric undulator field configuration is identified, which allows intense radiation of these harmonics. The power evolution in a free-electron laser (FEL) with such an undulator is studied by means of an analytical FEL model. The latter is enhanced by a true description of the gradual power saturation of harmonics. A FEL with elliptic undulator and electron–photon phase-shifting is proposed and modeled. It is shown that the resulting harmonic power from the phase-shifted elliptic undulator can be significantly higher than from a planar undulator with the same phase-shifting.

1. Introduction

In the 21st century, theoretical studies of undulator radiation (UR) remain important, especially regarding free-electron lasers (FELs) (McNeil & Thompson, 2010; Pellegrini *et al.*, 2016; Huang & Kim, 2007; Saldin *et al.*, 2000; Bonifacio *et al.*, 1984; Schmüser *et al.*, 2014; Pellegrini, 2016; Margaritondo & Ribic, 2011; Margaritondo, 2017). Notwithstanding fast development of numerical methods and computational facilities during the last decades, analytical studies preserve their value because they usually allow deeper insight into the underlying physics. UR theory involves generalized forms of Bessel and Airy functions, which accurately describe the radiation from relativistic charges in multi-periodic undulator magnetic fields. Analytical expressions for the UR in planar and spiral undulators involve relatively simple Bessel-type special functions; the exact description of the radiation in complex magnetic fields, consisting of multi-periodic and non-periodic components, remains a complicated mathematical problem. Analytical results for the UR in planar multi-component magnetic fields have been obtained by various authors (see, for example, Zhukovsky, 2015*a,b,c*, 2016*a,b*, 2017, 2018*a,b*, 2019*a*; Dattoli *et al.*, 2003, 2006; Zhukovsky & Potapov, 2017; Jia, 2011; Jeevakhan & Mishra, 2011; Mishra *et al.*, 2009; Zhukovsky & Kalitenko, 2019*a*); they involve complicated mathematical generalizations of the Bessel



functions and some conclusions, even for a two-frequency planar undulator, contradicting each other in various cases. Early works (Zhukovsky, 2015a, 2016a, 2018a; Dattoli *et al.*, 2003, 2006; Zhukovsky & Potapov, 2017; Jia, 2011) contained misprinted expressions and conclusions for the Bessel coefficients of planar bi-harmonic undulators, that were corrected later (Zhukovsky & Kalitenko, 2019a; Zhukovsky, 2019a,b). In the following we develop exact analytical expressions for the spontaneous and the stimulated undulator radiation intensities in the general case of a two-dimensional multi-periodic undulator magnetic field, which accounts for off-axis deviation and for the harmonic components in both spatial dimensions, present in real installations (see, for example, Ratner *et al.*, 2011; Lee *et al.*, 2015). Their numerical treatment through the solution of a system of equations for the fields and charges is very complicated; as far as we know, there are no user-ready computer programs for FEL radiation from an arbitrary two-dimensional periodic magnetic field with harmonics. Proper software is usually written *ad hoc* for the given specific field; its development is time- and cost-consuming and it requires proper computational environment and trained personnel. In the following we present analytical formulae of the generalized Bessel and Airy functions, which, in contrast to the numerical treatment, yields immediate results for the UR spectrum, and spontaneous and stimulated radiation intensities in the two-dimensional multi-periodic magnetic field of arbitrary intensity. In the limiting cases of the helical and planar undulators with field harmonics, they reduce to simpler expressions, which can be verified numerically and by comparison with FEL experiments (see Zhukovsky & Kalitenko, 2019a; Zhukovsky, 2019a). Our analytical results for the spontaneous UR intensities in multi-harmonic undulators were verified upon comparison with the reported experimental data by Lee *et al.* (2015) and, in some limiting cases, with the numerical results of the *SPECTRA* program (Tanaka, 2014; Tanaka & Kitamura, 2001; Kalitenko & Zhukovskii, 2020). We identify the field of the undulator with harmonics, advantageous for generating third and fifth FEL harmonics. We show that this potentially allows obtaining X-ray radiation from relatively low energy beams with the relativistic factor $\gamma \simeq 10^3$ in relatively compact installations of length ~ 30 m. Modeling of the radiation from single-pass FELs is performed with the phenomenological model (Zhukovsky & Kalitenko, 2019b,c; Zhukovsky, 2019c), which is based on the semi-analytical description of the FEL power evolution (Dattoli & Ottaviani, 2002; Dattoli *et al.*, 2004), and includes multi-stage saturation (Zhukovsky, 2019d) and power oscillations, verified by Zhukovsky (2020a,b,c) with a number of FEL experiments with reported harmonics. With its help, we obtain an analytical description of the FEL harmonic power along the whole undulator length.

2. Radiation from multi-harmonic undulators

Consider the following general configuration of the multi-periodic magnetic field in the undulator with multiple periods and main period $\lambda_{u,x}$,

$$\mathbf{H} = H_0 [\sin(k_\lambda z) + d \sin(pk_\lambda z), d_1 \sin(hk_\lambda z) + d_2 \cos(lk_\lambda z), 0],$$

$$k_\lambda = 2\pi/\lambda_{u,x}, \quad d, d_1, d_2 \in \text{real}, \quad h, l, p \in \text{integer}. \quad (1)$$

In the following we denote $\lambda_{u;x} \equiv \lambda_u$ for conciseness. We compute the radiation integral

$$\frac{d^2 I}{d\omega d\Omega} = \frac{e^2}{4\pi^2 c} \left| \omega \int_{-\infty}^{\infty} dt [\mathbf{n} \times [\mathbf{n} \times \boldsymbol{\beta}]] \exp[i\omega(t - \mathbf{nr}/c)] \right|^2 \quad (2)$$

for an electron in the relativistic limit, expanding the exponential and the integrand in the series of the small parameter $1/\gamma \ll 1$; \mathbf{n} is the unit-vector from the electron to the observer, \mathbf{r} is the electron radius-vector, $\boldsymbol{\beta}$ is its velocity, and c is the speed of light. The calculations of the radiation integral follow the general lines of Dattoli *et al.* (2006) and Zhukovsky (2015a,b,c, 2016a): the non-oscillating part of the exponential in the radiation integral yields the resonances for the UR and the periodic functions in the exponential of the integral naturally form the generalized Bessel functions. The account for axial asymmetry comes through the off-axis angle θ and the azimuthal angle φ , which are involved in the arguments of the following generalized Bessel function,

$$J_n^m(\xi_i) = \frac{1}{2\pi} \int_0^{2\pi} d\alpha \cos \left\{ n\alpha + \xi_1 \sin(h\alpha) + \xi_2 \cos(l\alpha) \right. \quad (3)$$

$$+ \xi_3 \sin \alpha + \xi_4 \sin(2\alpha) + \xi_5 \sin(2h\alpha) + \xi_6 \sin(2l\alpha)$$

$$+ \xi_7 \cos[(l+h)\alpha] + \xi_8 \cos[(l-h)\alpha] + \xi_9 \sin(p\alpha)$$

$$\left. + \xi_9 \sin[(p+1)\alpha] + \xi_{10} \sin[(p-1)\alpha] + \xi_{11} \sin(2p\alpha) \right\},$$

where the index m of the Bessel function $J_n^m(\xi_i)$ is determined by

$$\xi_4 = \frac{1}{4} \frac{mk^2}{1 + (k^2/2)[1 + (d/p)^2 + (d_1/h)^2 + (d_2/l)^2] + \gamma^2 \theta^2}, \quad (4)$$

where $k = H_0 \lambda_{u;x} e/2\pi m_e c^2$ is the main undulator parameter, θ is the off-axis angle, and azimuthal angle φ is involved in the following arguments,

$$\xi_0 = \frac{8d}{kp^2} \gamma \theta \sin \varphi \xi_4, \quad \xi_1 = \frac{8d_1}{kh^2} \gamma \theta \cos \varphi \xi_4, \quad (5)$$

$$\xi_2 = \frac{8d_2}{kl^2} \gamma \theta \cos \varphi \xi_4, \quad \xi_3 = \frac{8}{k} \gamma \theta \sin \varphi \xi_4,$$

$$\xi_5 = \frac{d_1^2}{h^3} \xi_4, \quad \xi_6 = -\frac{d_2^2}{l^3} \xi_4, \quad \xi_{11} = \frac{d^2}{p^3} \xi_4, \quad (6)$$

$$\xi_7 = \frac{4d_1 d_2}{hl(l+h)} \xi_4, \quad \xi_8 = \frac{4d_1 d_2}{hl(l-h)} \xi_4$$

$$\xi_9 = \frac{4d}{p(p+1)} \xi_4, \quad \xi_{10} = \frac{4d}{p(p-1)} \xi_4. \quad (7)$$

Formulae (3)–(7) are good for the arbitrary strengths of the field components in (1). In real devices, field harmonic amplitudes rarely reach $\sim 1/4$ of the main field; then proper arguments (5)–(7) simplify and so does the generalized Bessel

function (3). For example, for a planar undulator with field harmonics, $d/p, d_1/h, d_2/l \ll 1$ in (1), and the ratios $d_1^2/h^3, d_2^2/l^3, d^2/p^3$ etc. in (5)–(7) are small, so that the main contribution in $J_n^m(\xi_i)$ (3) comes from the terms $\xi_{3,4}$. Then the Bessel function (3) can be approximated by the following Bessel function of just two arguments, usual in UR studies,

$$J_n^m|_{\text{planar}}(\xi_i) \cong \tilde{J}_n(\zeta, \xi) = \frac{1}{2\pi} \int_0^{2\pi} \cos(n\alpha + \zeta \sin \alpha + \xi \sin 2\alpha) d\alpha, \quad (8)$$

where $\zeta = \xi_3, \xi = \xi_4$. For a helical undulator, $d_2 = l = 1$ and proper simplifications follow accordingly. The difference between the results (8) and (3) for odd harmonics is $<5\%$; the difference can be higher for even UR harmonics, but the latter are nevertheless weak.

For the undulator field (21) with multiple periods l, h, p , the resonance wavelengths of the UR are lower due to the terms $(d/p)^2 + (d_1/h)^2 + (d_2/l)^2$ in the following expression,

$$\lambda_n = \frac{\lambda_u}{2n\gamma^2} \left\{ 1 + \frac{k^2}{2} \left[1 + \left(\frac{d}{p}\right)^2 + \left(\frac{d_1}{h}\right)^2 + \left(\frac{d_2}{l}\right)^2 \right] + (\gamma\theta)^2 \right\}. \quad (9)$$

The intensity of the UR from an electron in the field (1) with harmonics reads as follows,

$$\frac{d^2I}{d\omega d\Omega} = \frac{e^2 N^2 \gamma^2 k^2 \sum_{n=-\infty}^{\infty} n^2 \text{sinc}^2(v_n/2) \left(|T_{n,x}|^2 + |T_{n,y}|^2 \right)}{c \left\{ 1 + (k^2/2) \left[1 + (d/p)^2 + (d_1/h)^2 + (d_2/l)^2 \right] + (\gamma\theta)^2 \right\}^2}, \quad (10)$$

where N is the number of main undulator periods, $v_n = 2\pi n N [(\omega/\omega_n) - 1]$ is the detuning parameter, describing the deviation from the resonances $\omega_n = 2\pi c/\lambda_n$, and $T_{n,x,y}$ are the amplitudes for the x - and y -polarizations of the radiation,

$$T_{n,x} = \frac{2}{k} \gamma\theta \cos \varphi J_n^n + \frac{d_1}{h} (J_{n+h}^n + J_{n-h}^n) + i \frac{d_2}{l} (J_{n+l}^n - J_{n-l}^n), \quad (11)$$

$$T_{n,y} = \frac{2}{k} \gamma\theta \sin \varphi J_n^n + (J_{n+1}^n + J_{n-1}^n) + \frac{d}{p} (J_{n+p}^n + J_{n-p}^n), \quad (12)$$

where $J_n^m \equiv J_n^m[\xi_i(m)]$ are the generalized Bessel functions (3). Their simplified forms, such as (8) for a planar undulator, can be used especially for the odd UR harmonics, if the field harmonic are weak. Despite the apparent complexity of (3)–(12), these formulae allow easy and fast computation of the spontaneous UR intensity and relevant Bessel factors with the help of any common software, such as *Mathematica*, *Matlab*, *Scientific Workplace*, or even a scientific calculator. Otherwise, the numerical study of the UR in the two-dimensional magnetic field with harmonics requires even more efforts and *ad hoc* development of proper software. Formulae (3)–(12) and their limiting cases can be coupled with the phenomenological FEL model (see Zhukovsky & Kalitenko, 2019b,c;

Zhukovsky, 2019c,d, 2020a,b,c), which is based on the approach of Dattoli & Ottaviani (2002) and Dattoli *et al.* (2004), to evaluate the single-pass FEL performance, as we will show in the following sections.

3. The effects of the electron energy spread, angular deviation and off-axis position on the UR

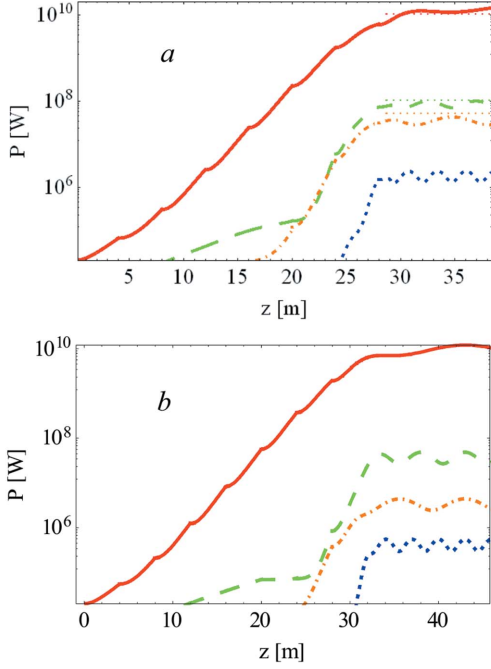
The electron energy spread, σ_e , is one of the major sources of losses in the UR. It can be accounted for analytically with the convolution

$$\int_{-\infty}^{\infty} \frac{d^2I(v_n + 4\pi n N \varepsilon)}{d\omega d\Omega \sqrt{2\pi} \sigma_e} \exp\left(-\frac{\varepsilon^2}{2\sigma_e^2}\right) d\varepsilon.$$

Relativistic beams in the modern FEL installations have very low energy spread, usually $\sigma_e \simeq 10^{-3}$ to 10^{-4} . Nevertheless, the variation within this range changes significantly the harmonic radiation intensities and the FEL saturation length. For example, the radiation of high harmonics in the LCLS FEL (Emma *et al.*, 2010; Ratner *et al.*, 2011; Emma, 2009) was observed from a beam with energy spread $\sigma_e \simeq 10^{-4}$; at PAL-XFEL (Kang *et al.*, 2017) with similar radiation wavelengths ~ 0.15 nm and ~ 1.5 nm the harmonics were not registered. One of many reasons for that, and arguably the main one, was the significantly higher energy spread in the POHANG FEL, $\sigma_e \simeq 1.8 \times 10^{-4}$ to 5×10^{-4} (Kang *et al.*, 2017), than that in the LCLS FEL; the weak condition for the Pierce parameter, $\rho > 2\sigma_e$, was hardly fulfilled for the fundamental tone; for high harmonics the inequality was not fulfilled: $\rho < \sigma_e$. Another installation, SWISS FEL (Milne *et al.*, 2017), has very low absolute energy spread, 350 keV, which translates into $\sigma_e = 0.006\%$ for the energy $E = 5.8$ GeV. The harmonic power evolution is shown in Fig. 1(a); for the third harmonic we obtain 1% content and for the second harmonic 0.5% of the fundamental [thin dotted lines in the saturation region in Fig. 1(a)]. A higher spread, $\sigma_e = 0.018\%$, like that in PAL-XFEL, effects the harmonic power noticeably as shown in Fig. 1(b).

Further increase of the energy spread increases the gain length and the saturation length, and decreases the fundamental power; high harmonics become very weak. The study was performed analytically, using the phenomenological FEL model (Zhukovsky, 2019d, 2020a,b,c) with enhanced description of the harmonic behaviors around saturation.

In real undulators, there can be some non-periodic magnetic constituents due to magnetizing errors in undulators and due to the external effects, for example the magnetic field of the Earth. The respective field integrals are carefully evaluated and the undesired fields are compensated or screened out by magnetic shimming. We provide an analytical description of the possible effect of such non-periodic fields H_d , which bend the electron trajectory in the effective angle θ_H . Omitting the details, we note that evaluation of the radiation integral for a charge in a periodic magnetic field with a constant component yields additional non-periodic terms in the exponential of the


Figure 1

Harmonic power evolution at SWISS XFEL; (a) the energy spread 350 keV for $E = 5.8$ GeV represents the real installation; (b) the assumed spread is three times higher: $\sigma_e = 0.018\%$. Harmonics: $n = 1$, red solid; $n = 2$, orange dot-dashed; $n = 3$, green dashed; $n = 5$, blue dotted line.

integral. Collected together, they form the following generalized Airy-type function,

$$S(\nu_n, \beta, \eta) \equiv \int_0^1 d\tau \exp \left\{ i \left[\tau \nu_n + \tau^2 \frac{(2\pi N)^2 \gamma \theta}{1 + k^2/2} n k (\kappa \cos \phi - \rho \sin \phi) + \tau^3 \frac{2\pi N n (\gamma \theta_H)^2}{1 + k^2/2} \right] \right\}, \quad (13)$$

where ν_n is the detuning parameter,

$$\gamma \theta_H = \frac{2\pi}{\sqrt{3}} \frac{H_d}{H_0} k N = \frac{107.1 \sqrt{3} H_d [\text{G}]}{2\pi L_u [\text{m}]}$$

is the effective bending angle, induced by the non-periodic magnetic components $H_{d,x} = \rho H_0$, $H_{d,y} = \kappa H_0$. This induced angle $\gamma \theta_H$ is accumulated along the undulator length $L_u = \lambda_u N$ and it modifies the angular part of the expressions for the UR resonances and the UR intensity: $\theta^2 \rightarrow \Theta^2 = \theta^2 + \theta_H^2 - \sqrt{3} \theta_H \theta (\rho \sin \phi - \kappa \cos \phi) (H_0/H_d)$. The shape of the spectral line is described by the generalized function S and its derivative $\partial S/\partial \nu_n$,

$$|T_n|^2 \text{sinc}^2(\nu_n/2) \rightarrow |T_n S|^2 + |\bar{T}_n \partial S/\partial \nu_n|^2, \quad (14)$$

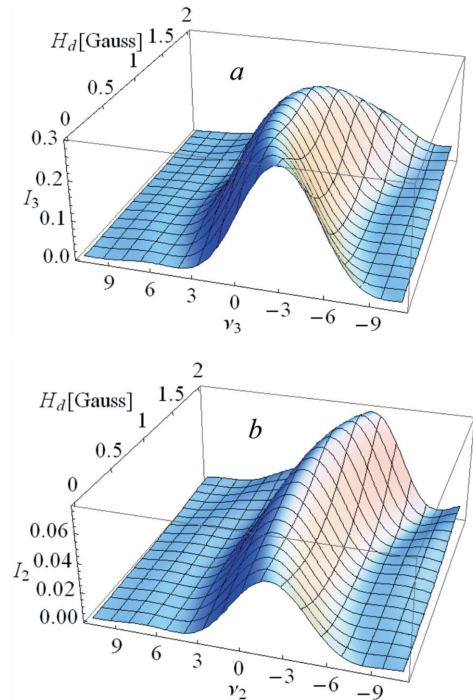
where the term \bar{T}_n arises from the non-periodic magnetic component H_d ,

$$\bar{T}_n = 2\sqrt{3} \gamma \theta_H J_n^n/k. \quad (15)$$

Note that the constant field H_d gives rise to the even harmonics of the spectrum on the axis, which is shown by \bar{T}_n (15). The properties of the generalized Airy functions will be

explored in detail elsewhere; we note here that $\max[S] = 1$, $\max[\partial S/\partial \nu_n] = 0.5$ and S reduces to the common sinc function for $\eta = \beta = 0$: $S(\nu_n, 0, 0) = \exp(i\nu_n/2) \text{sinc}(\nu_n/2)$. This, taking into account the coefficient 2 in (15), yields the contribution similar to that of the first terms in (11), (12) upon the substitution $\theta \rightarrow \theta_H$ in them. These angular contributions, however, come from different angles. The possible effect of the constant field of the Earth on the radiation on the LCLS FEL was mentioned by Emma *et al.* (2010). It was screened out to avoid the distortion of the UR lines, and rigorous controls after each undulator section were performed. We reconstruct theoretically the possible distortions with regard to the spontaneous UR as shown in Figs. 2 and 3. For the FEL radiation, this translates through the Pierce parameter into a stronger second FEL harmonic and slightly weaker third and fifth harmonics of the spectrum.

Note that the effect of the angles θ_H and θ can be mutually opposite, and they can compensate each other; this means that the resonance condition, corresponding to zeroes of the phase of the exponential in (13), can be satisfied for $\nu_n \simeq -(\beta + \eta)$. For example, for the third UR harmonic of the LCLS undulator (Emma *et al.*, 2010) the infrared shift of the radiation in the angle $\gamma \theta = 0.1$ can be best compensated by the magnetic field $H_d \simeq 1$ G (see Fig. 2). In a long undulator, such as LCLS, where $L = 3.4$ m, the angle $\gamma \theta_H \simeq 0.1$, which causes noticeable distortion, can be induced by a relatively weak field, as compared with the undulator field amplitude ~ 1 T. Indeed, $H_d \simeq 1$ G causes $\gamma \theta_H \simeq 0.1$ in the LCLS undulator and this displaces the electron transversally in ~ 10 – 20 μm on one gain


Figure 2

Spectral line of the third (a) and of the second (b) FEL harmonics of the LCLS undulator with period $\lambda_u = 3$ cm, $k = 3.5$, $N = 113$, $\sigma_e = 0.0003$, $\gamma = 8400$, off-the-axis angle $\gamma \theta = 0.1$. The spectral lines are shown for the detuning parameter ν_n and the field H_d .

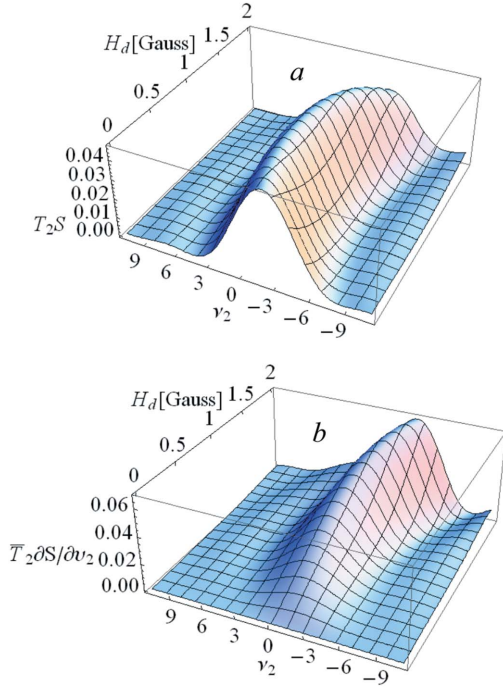


Figure 3
Contributions of the off-axis angle $\gamma\theta = 0.1$ (a) and of the non-periodic field H_d (b) to the spectral line of the second UR harmonic of the LCLS undulator, $\lambda_u = 3$ cm, $k = 3.5$, $N = 113$, $\sigma_e = 0.0003$, $\gamma = 8400$ for the detuning parameter ν_n and the field strength H_d .

length ($L_g \simeq 1.5\text{--}3.5$ m dependent on the experiment), by far exceeding the target alignment, $5\ \mu\text{m}$, of the beam in the undulators (Emma *et al.*, 2010). This shows why in real devices the non-periodic fields are avoided and carefully compensated.

For the second UR harmonic we show the contributions of the off-axis angle $\gamma\theta = 0.1$ and of the non-periodic field H_d in Figs. 3(a) and 3(b), respectively. The second harmonic was registered with noticeable power and reported by Emma (2009). The comprehensive result for the second harmonic is demonstrated in Fig. 2(b).

The off-axis position y_0 of the electron in the beam, whose transversal size is $\sigma_{x,y}$, also causes another well known effect – betatron oscillations. They cause the split of the spectral lines and give rise to even-harmonics radiation on the undulator axis. This topic has been recently readdressed by Prakash *et al.* (2016) with regard to the bi-harmonic undulator. For the undulator with multi-harmonic field (1) we obtain similar results, which reduce in their limiting cases to those of Prakash *et al.* (2016). The split of the UR line occurs in the harmonics, distant by the betatron frequency,

$$\omega_\beta = \frac{\sqrt{2}\pi c k \delta}{\lambda_n n \gamma} \quad (16)$$

$$= \frac{2\sqrt{2}\pi c \gamma k \delta}{\lambda_u \{1 + (k^2/2)[1 + (d/p)^2 + (d_1/h)^2 + (d_2/l)^2] + (\gamma\Theta)^2\}}$$

where $\delta = 1$ for a common planar undulator and $\delta = (1 + d^2 + d_1^2 + d_2^2)^{1/2}$ for the field (1). For ultra-relativistic electrons, $\gamma \gg 1$, we obtain

$$\omega_\beta \ll \omega_n \simeq \frac{4\pi c n \gamma^2}{[1 + (k^2/2)] \lambda_u},$$

$$\frac{\omega_\beta}{\omega_n} \simeq \frac{k \delta}{\sqrt{2} n \gamma} \propto \frac{1}{\gamma}.$$

In X-ray FELs the relativistic factor of the beams is very high, $\gamma \simeq 10^3$ to 10^4 , and the spectral line split is very small: $\sim 1/\gamma$. This split of radiation lines in p harmonics is described by the series of the Bessel functions in (11) and (12), factorized by $\tilde{J}_p(\zeta, \xi)$ (8),

$$T_n \rightarrow \sum_p T_n \tilde{J}_p(-\zeta, -\xi), \quad (17)$$

where

$$\zeta = \frac{2\pi\theta y_0}{n\lambda_n} = \frac{4\pi\theta y_0 \gamma^2}{\lambda_u [1 + (k^2/2)]}, \quad (18)$$

$$\xi = \frac{\pi^2 y_0^2 k \delta}{2n\gamma \sqrt{2} \lambda_u \lambda_n} = \frac{\pi^2 \gamma y_0^2 k \delta}{\sqrt{2} \lambda_u^2 [1 + (k^2/2)]}.$$

The split regards also the even harmonics due to the initial off-axis position of electrons in the beam. Their respective additional term in (10) reads as follows,

$$\tilde{T}_n \simeq \sqrt{2}\pi d \frac{y_0}{\lambda_u} \sum_p J_n^n(\xi_i) [\tilde{J}_{p+1}(-\zeta, -\xi) - \tilde{J}_{p-1}(-\zeta, -\xi)], \quad (19)$$

where $\tilde{J}_p(\zeta, \xi)$ is defined by (8) and depends on ζ, ξ (18), and $J_n^n(\xi_i)$ is defined by (3) for the undulator field (1); the result in the limiting case of the bi-harmonic undulator reduces to that of Prakash *et al.* (2016). The contribution of the betatron oscillations to the even harmonic generation is rather small. In practical terms $\tilde{T}_{n=2,4} \simeq 0.01$; this is usually comparable with the contribution of the divergence angle of the beam in (11), (12). In comparison, other terms in (11), (12) are larger: $T_{n=1} \simeq 0.75$, $T_{n=3} \simeq 0.3$, $T_{n=5} \simeq 0.15$, $T_{n=2} \simeq \tilde{T}_{n=2} \simeq 0.05\text{--}0.1$.

While the even harmonics due to the betatron oscillations are weak, another effect of the beam size is appreciable. Indeed, the split of a radiation line in many harmonics may occur even in the installations with narrow electron beams and it can be measured. Employing the above-developed formalism of special functions, we studied analytically the spectrum lines of several installations. For example, for the LCLS FEL (Emma *et al.*, 2010), where the beam size is $\sigma_{x,y} \simeq 20\text{--}30\ \mu\text{m}$, the fundamental line is split into a few harmonics: in soft X-rays the fundamental at $\lambda = 1.5$ nm is split into ~ 5 harmonics [see Fig. 4(a)]; in hard X-rays, the fundamental at $\lambda = 0.15$ nm is split into ~ 10 harmonics as shown in Fig. 4(b). They yield the theoretical spectral density $\Delta\lambda/\lambda \simeq 0.1\%$, in agreement with the design value of Emma *et al.* (2010). In comparison, we present in Fig. 5 the spectral lines of the PAL-XFEL (Kang *et al.*, 2017), which has the same radiation wavelengths as LCLS, similar undulators, but poorer quality beam with higher energy spread for hard X-rays, and some larger emittances and wider beams.

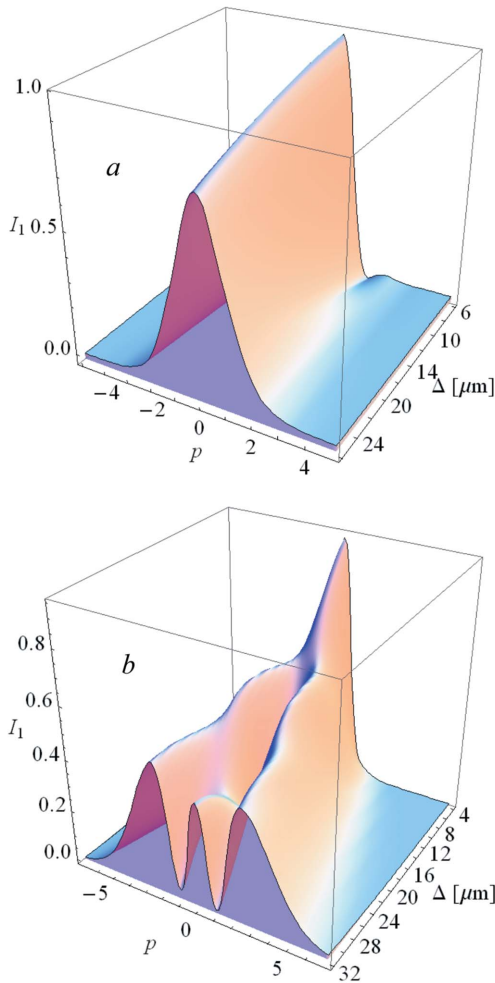


Figure 4
Split of the fundamental radiation line in betatron harmonics p for LCLS FEL at $\lambda = 1.5$ nm (a) and at $\lambda = 0.15$ nm (b) as a function of the distance from the axis Δ .

The resulting theoretical line split for PAL-XFEL is more significant than that for LCLS, as follows from comparison of Figs. 5 and 4. However, due to a smaller value of the undulator parameter $k = 1.87$ in PAL-XFEL versus $k = 3.5$ in LCLS, the betatron harmonics of the fundamental line are roughly twice as close to each other, $\omega_\beta/\omega_1 = k/(\gamma\sqrt{2})$, for the PAL-XFEL than for the LCLS line, and the estimate of the spectral width is similar, $\Delta\lambda/\lambda \simeq 0.1\%$. The split of the fundamental spectrum line at SWISS XFEL (Milne *et al.*, 2017) at $\lambda = 0.1$ nm, where the beam has the same transversal size $\sigma_{x,y} \simeq 25$ μm , is shown in Fig. 6(a).

The split is noticeable, but well contained. The computations of the theoretical spectral density give $\Delta\lambda/\lambda \simeq 0.1\%$; this is in the reported range 0.05–0.15% (Abela *et al.*, 2017). The spectral line of the LEUTL FEL (Milton *et al.*, 2001) in the UV-A range at $\lambda_1 = 385$ nm is generated by a wide beam with transversal size $\sigma_{x,y} \simeq 0.25$ mm. One would expect significant betatron oscillations and their influence, including strong even harmonics and line split. However, the second harmonic registered in this experiment comes mostly due to the large angle of photon–electron interactions in the wide electron

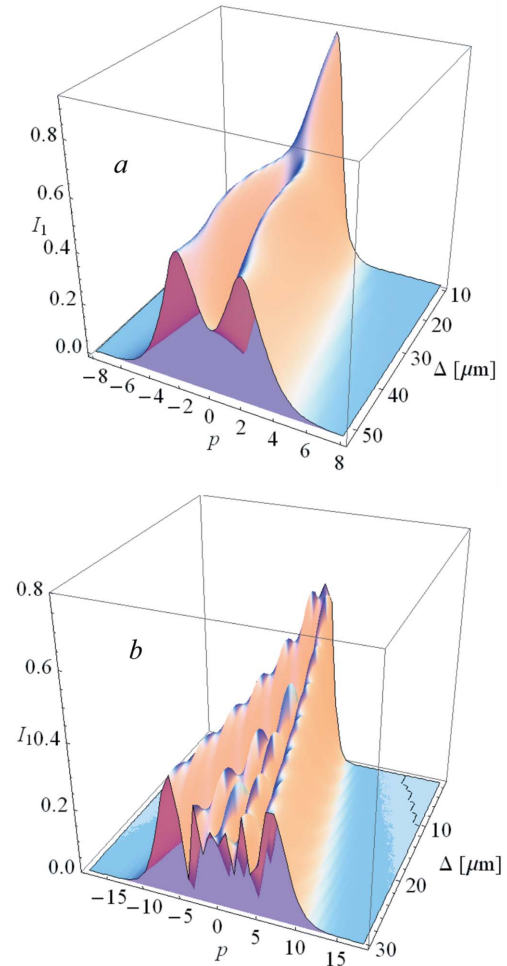


Figure 5
Split of the fundamental radiation line in betatron harmonics p for PAL XFEL at $\lambda = 1.5$ nm (a) and at $\lambda = 0.144$ nm (b) as a function of the distance from the axis Δ .

beam (Zhukovsky, 2020a,c). The contribution of the betatron oscillations and the off-axis position of the electrons to the even UR harmonics is low: proper Bessel coefficients of the angular part, $T_{2,4}$, exceed the betatron terms $\tilde{T}_{2,4}$ by an order of magnitude. The fundamental line of the LEUTL FEL consists of a few betatron harmonics [see Fig. 6(b)]. Accounting for them, we obtain the width $\Delta\lambda \simeq 3.5$ nm in agreement with the data of Milton *et al.* (2001) in the exponential power growth. Close to the saturation the theoretical relative bandwidth is approximately $\lambda[\rho/(L_s/\lambda_u)]^{1/2} \simeq 0.2\% \simeq \rho$, and the coherence time is $\tau_c \simeq \lambda^2/c\Delta\lambda \simeq 0.5$ ps. Then for the electron bunch of duration $\tau_e \simeq 0.65$ ps, one coherence region fits and one mode is radiated (Milton *et al.*, 2001).

4. Effect of the magnetic field harmonics on the UR

The limiting case of the field (1), where $d_1 = d_2 = 0$, describes the planar undulator with the field harmonic $H = H_0[\sin(k_\lambda z) + d \sin(hk_\lambda z)]$. It has been analytically and numerically studied in many works (for example Zhukovsky & Kalitenko, 2019a,c;

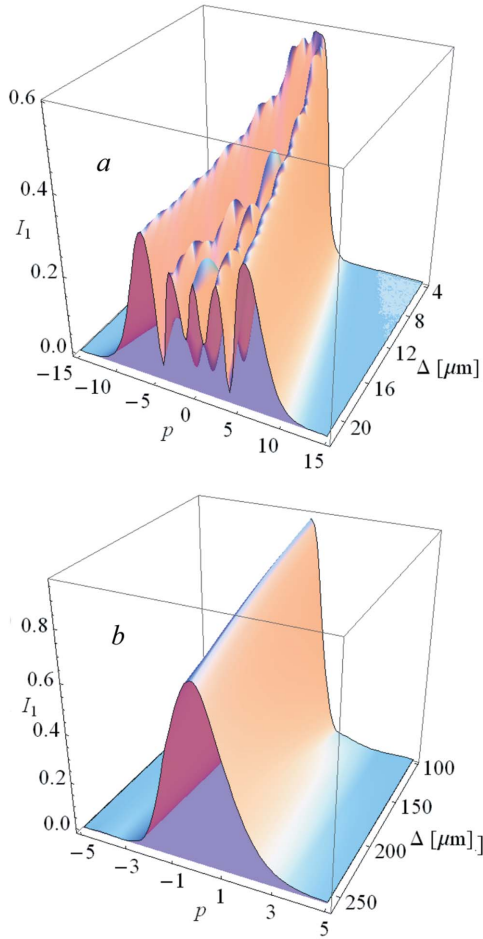


Figure 6 Split of the fundamental radiation line in betatron harmonics p at SWISS FEL at $\lambda = 0.1$ nm (a) and at LEUTL FEL at $\lambda = 385$ nm (b) as a function of the distance from the axis Δ .

Zhukovsky, 2019a,c,e; Prakash *et al.*, 2016). The radiation wavelengths

$$\lambda_n \cong \frac{\lambda_u}{2n\gamma^2} \left\{ 1 + \frac{k^2}{2} \left[1 + \left(\frac{d}{h} \right)^2 \right] + (\gamma\theta)^2 \right\}$$

and intensities follow straight from formulae (9) and (10), which are more general. A comparison of the normalized UR intensities taking into account the third field harmonic with the numerical results of *SPECTRA* software (Tanaka, 2014; Tanaka & Kitamura, 2001) showed very good agreement for all harmonics (Kalitenko & Zhukovskii, 2020). In the following we consider various undulators and installations with electron energies over a wide range and we compare our theoretical results with the available experimental data for real devices.

We demonstrate the effect of the strong third field harmonic with amplitude dH_0 on the radiation of a planar undulator [$d_1 = d_2 = 0$ in (1)], where H_0 is the undulator main field intensity; the results are shown in Fig. 7(a) for $d = -0.4$ and in Fig. 7(b) for $d = +0.4$. The electron beam characteristics are of the SPARC installation (Giannessi *et al.*, 2011); we assume an electron energy $E_e = 152$ MeV, energy spread $\sigma_e = 10^{-3}$,

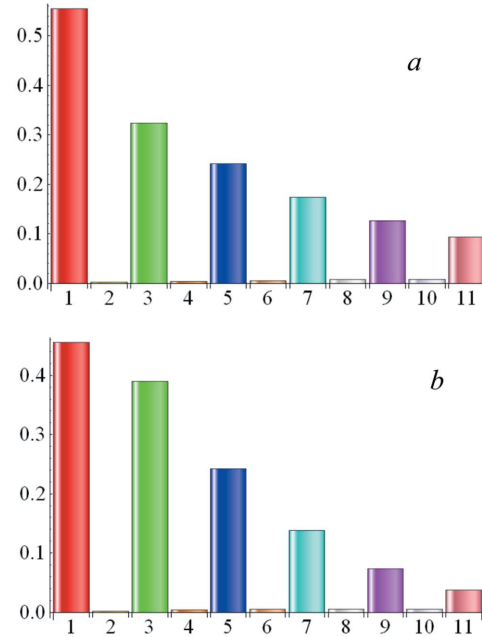


Figure 7 UR harmonic intensities in the planar undulator with $k = 2.133$, $h = 3$, $\sigma_e = 10^{-3}$ in relative units versus the harmonic number n [(a) $d = -0.4$; (b) $d = +0.4$].

relativistic factor $\gamma = 297$, electron beam power $P_E = 8$ GW, beam current $I_0 = 53$ A, current density $J = 4.35 \times 10^8$ A m⁻², full beam section $\Sigma = 1.22 \times 10^{-7}$ m², normalized emittance $\varepsilon^n = 2.7$ mm mrad, Twiss parameter $\beta = 2.2$ m, undulator parameter $k = 2.133$, and undulator period $\lambda_u = 2.8$ cm. The computations were made for $N = 150$ periods. Here and in the following the harmonics in the plots are color-coded: $n = 1$, red; $n = 2$, orange; $n = 3$, green; $n = 4$, yellow; $n = 5$, blue lines and bars.

For $d = -0.4$ the fundamental tone, $n = 1$, and the harmonics with $n = 7, 9, 11$ etc. are stronger, while the third harmonic is weaker as compared with their intensities for $d = +0.4$ [see Fig. 7(a)]. For $d = +0.4$ [see Fig. 7(b)] we see some stronger third UR harmonic and weaker first, seventh, ninth and eleventh harmonics; the fifth UR harmonics are practically not affected; for a detailed study of the effect of the third field harmonic on the UR, see Zhukovsky (2019a,c,e).

Analytical expressions for the particular case of the UR from the helical undulator, whose magnetic field contains the following anti-symmetric field harmonics,

$$\mathbf{H} = H_0 [\sin(k_\lambda z) - d \sin(hk_\lambda z), \cos(k_\lambda z) + d \cos(hk_\lambda z), 0], \quad h \in \text{integers}, \quad (20)$$

were presented by Zhukovsky (2019a,c). We calculated the UR from an electron in the field (20) with the third field harmonic accounting for the beam asymmetry and finite size; for example, the results for $h = 3$, $d = 0.0825$ and $d = 0.3$ are shown in Fig. 8.

The presence of the third field harmonic with the field (20) was reported by Lee *et al.* (2015), where the helical undulator with period $\lambda_u = 2.3$ cm, $N = 30$ and $k = 2.21622$ was described.

We assume the data of this device (Lee *et al.*, 2015) and the reported field (20) with amplitude $H_0 = 9.7$ kG, $d = 0.0825$, $h = 3$, $dH_0 = 0.8$ kG, relativistic factor $\gamma = 12.72$, electron beam energy $E = 6.5$ MeV, emittances $\varepsilon_x = 1.5$ mm mrad and $\varepsilon_y = 0.35$ mm mrad, beta functions $\beta_x = 43.66$ cm and $\beta_y = 28.75$ cm, beam sections $\sigma_x = 809$ μm and $\sigma_y = 317$ μm , and divergences $\theta_x = 4.5$ mrad and $\theta_y = 1.6$ mrad (see Lee *et al.*, 2015). With the above data, we calculate the radiated on-axis harmonic UR intensity separately for x - and y -polarizations accounting for the axial asymmetry of the beam, using the generalized Bessel functions, and obtain the results shown in Fig. 8(a). In the ideal helical undulator with the ideal beam only the fundamental tone (red bar) would be radiated on the axis. In reality more UR harmonics appear. The second harmonic (short orange bar) is $\sim 1.5\%$ of the fundamental (see Fig. 8); the power of the fifth UR harmonic is $\sim 2\%$ of the fundamental for $d = 0.0825$ and it is much stronger than the third UR harmonic in agreement with experiment (Lee *et al.*, 2015). Stronger even harmonics in y -polarization than in x -polarization are due to higher divergence θ_x than θ_y ; it also slightly decreases the intensity of odd harmonics in y -polarization. Thus, the asymmetry of the electron beam, accounted for analytically, causes some difference in the harmonic content for x - and y -polarizations, shown in Fig. 8. The third field harmonic gives rise to the fifth UR harmonic (blue bar) in the radiation spectrum. The third UR harmonic is suppressed and the fifth is enhanced due to the anti-symmetry of the third field harmonic d in (20); d has opposite signs in the x - and y -polarizations. The electron energy spread expectably broadens the UR lines and

decreases the UR intensity; it can be demonstrated graphically, similarly to that given by Zhukovsky (2015a,b,c, 2016a,b, 2017, 2018b), Zhukovsky & Potapov (2017), Jia (2011), Jeevakhan & Mishra (2011) and Mishra *et al.* (2009); we omit the plots for conciseness. Comparison of the plots in Figs. 8(a) and 8(b) show that the stronger third field harmonic dH_0 [see (20)] of the main undulator magnetic field increases the radiation of high UR harmonics, especially the fifth (blue lines in Fig. 8): for $d = 0.3$ the fifth UR harmonic is $\sim 25\%$ of the fundamental for the low energy spread $\sigma_e = 1 \times 10^{-4}$ [see Fig. 8(b)]. Higher energy spread, $\sigma_e = 1 \times 10^{-3}$, naturally reduces the fifth UR harmonic to $\sim 8\%$ of the fundamental, and even higher spread, $\sigma_e > 1 \times 10^{-3}$, is even more detrimental.

Modeling of the FEL with the elliptic undulator (20) with anti-symmetric third field harmonics was performed by Zhukovsky (2019a,c); we hoped for a rather strong fifth FEL harmonic, but the results demonstrated that it was barely noticeable on the background of the initial shot noise, while the third harmonic was suppressed by the field configuration. Therefore, the anti-symmetric field (20) does not represent particular interest for FEL harmonic generation. Now we consider the following asymmetric elliptic undulator magnetic field,

$$\mathbf{H} = H_0 [\sin(k_\lambda z), d_2 \cos(lk_\lambda z) + d_1 \sin(hk_\lambda z), 0], \quad l \neq h, \quad l, h \in \text{integers}, \quad (21)$$

with period $\lambda_{u,x} \equiv \lambda_u$, $k_\lambda = 2\pi/\lambda_u$ along the x -coordinate, $\lambda_{u,y}^1 = \lambda_u/h$ and $\lambda_{u,y}^2 = \lambda_u/l$ along the y -coordinate; (21) can be viewed as an elliptic undulator field with an additional periodic field component in one plane. We assume multiple periods and $l \neq h$ to study the field harmonics effect in this undulator. In the limiting cases, $d_1 = 0, d_2 \neq 0$ and $d_1 \neq 0, d_2 = 0$, the field (21) simplifies and describes simpler elliptic undulators [see, for example, Zhukovsky (2019c)]; for $d_1 = 0, d_2 = 1$ and $l = 1$ we obtain common helical undulator with $f_{1;x,y} = 1, f_{n \neq 1} = 0$, where, ideally, only the fundamental tone is radiated on the axis. For $d_1 = 1, d_2 = 0$ and $h = 1$, we obtain the planar undulator with the parameter $k_{\text{eff}} = \sqrt{2}k$ and the polarization turned 45° .

Let us analyze the UR in the field (21) and identify the best values of d_1, d_2, h for high UR harmonic generation. Along the x -axis the common sinusoidal field is present in (21) just like in any planar undulator; along the y -axis we have the combination of periodic sin and cos magnetic fields with multiple periods and arbitrary amplitudes. Since (21) is actually the limiting case of (1) for $d = 0$, rigorous analytical calculations for the UR in the field (21) unsurprisingly yield formulae (3)–(12), where $d = 0$ must be assumed. In real devices the normalized angle $\gamma\theta$ usually has the order of 10^{-2} and thus the term $(\gamma\theta)^2$ is small compared with unity and with k^2 . The radiation of the undulators is mostly determined by the first and the third field harmonics [see, for example, Alexeev & Bessonov (1991)], so we study the effect of the third field harmonic in the following. Let us consider $h = 3, l = 1, d_1 = 1, d_2 = 0.25$, *i.e.* the magnetic field

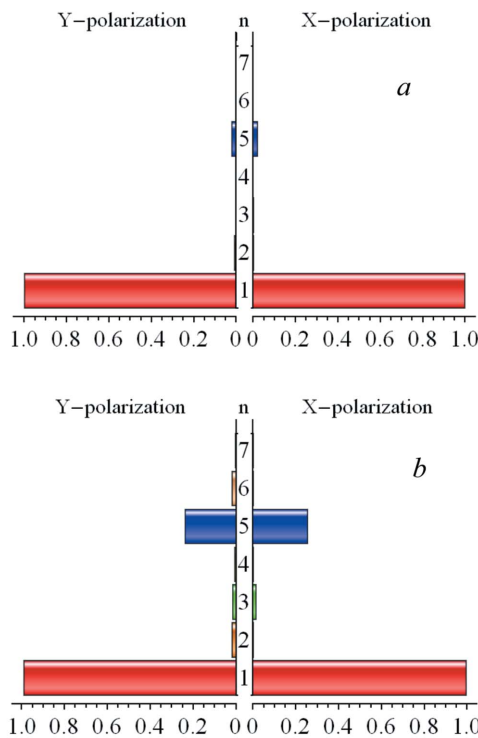


Figure 8 On-axis UR harmonics intensity (in relative units) from the elliptic anti-symmetric undulator (20) for $k = 2.21622$, $d = 0.0825$ (a) and $d = 0.3$ (b); the energy spread is $\sigma_e = 10^{-4}$.

$$\mathbf{H} = H_0[\sin(k_\lambda z), 0.25 \cos(k_\lambda z) + \sin(3k_\lambda z), 0], \quad (22)$$

which describes an asymmetric undulator with the third field harmonic along the y -axis. The resulting UR possesses rather interesting features, such as the intense radiation of high harmonics. To be able to compare the radiation in the field (22) with that of the helical undulator with field harmonics (see Fig. 8), we assume the same low-energy beam of the test installation (Lee *et al.*, 2015) with relativistic factor $\gamma = 12.72$ (see the details in Section 2), undulator parameter $k = 2.21622$ and period $\lambda_u = 0.023$ m in (22), as we did for the undulator field (20). The spectrum of the UR from an electron in the field (22), however, is very different from that in the field (20). We obtain the following values for the Bessel coefficients $f_{n,x}, f_{n,y}$,

$$f_{x;n=1,\dots,9} = \{0.292, 0.023, 0.280, 0.011, 0.217, 0.010, 0.144, 0.011, 0.096\}, \quad (23)$$

$$f_{y;n=1,\dots,9} = \{0.795, 0.003, 0.388, 0.003, 0.191, 0.004, 0.104, 0.004, 0.068\}. \quad (24)$$

Note in (23) that the Bessel coefficients for the fundamental harmonic in x -polarization and for the third harmonic are almost the same, $f_{x;1} \simeq 0.29$, $f_{x;3} \simeq 0.28$, and the Bessel coefficient for the fifth harmonic, $f_{x;5} \simeq 0.22$, is comparable with $f_{x;1}$ and $f_{x;3}$. The intensities of the UR harmonics in x -polarization [top plot (a)] and y -polarization [bottom plot (b)] accounting for the energy spread $\sigma_e = 10^{-4}$ are shown in Fig. 9. The

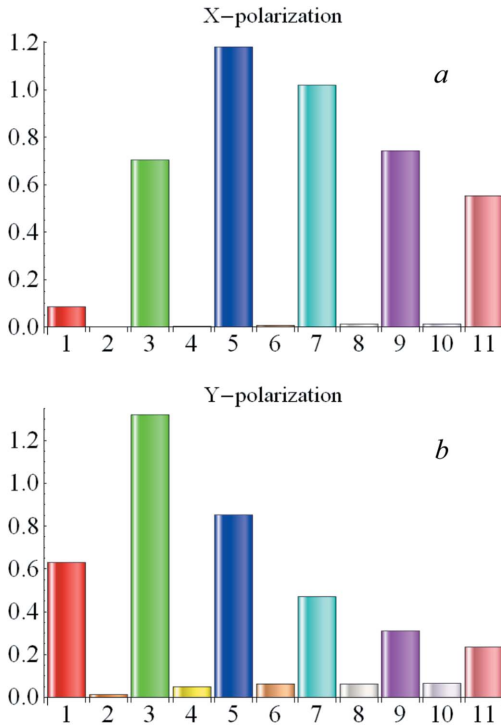


Figure 9 On-axis UR harmonics intensity (in relative units) for the elliptic undulator with $k = 2.21622$, $h = 3$, $d_1 = 1$, $d_2 = +0.25$, $l = 1$, $\sigma_e = 10^{-4}$, $N = 30$; x -polarization (a); y -polarization (b).

spectrum in Fig. 9 is indeed very different from that of the helical undulator with field harmonics (compared with Fig. 8): we observe in Fig. 9(a) that the x -polarized third and fifth UR harmonics are stronger by one order of magnitude than the fundamental tone of this polarization and this can be exploited in FELs. Although the high harmonics become weaker for higher energy spread, the fifth harmonic still remains three times stronger than the fundamental for $\sigma_e = 10^{-3}$. Also in y -polarization, the third UR harmonic is stronger than the fundamental [see Fig. 9(b)].

Thus, the third and fifth UR harmonics prevail in the UR spectrum of electrons in the undulator field (22). The difference in even harmonic content between the polarizations is caused by both the asymmetric beam and the undulator.

For the suppressed periodic cos component we set, for example, $d_2 = 0.01$ in (21),

$$\mathbf{H} = H_0[\sin(k_\lambda z), 0.01 \cos(k_\lambda z) + \sin(3k_\lambda z), 0]. \quad (25)$$

Then we obtain the following Bessel coefficients for this undulator,

$$f_{x;n=1,\dots,9} = \{0.059, 0.003, 0.244, 0.001, 0.183, 0.001, 0.121, 0.002, 0.087\}, \quad (26)$$

$$f_{y;n=1,\dots,9} = \{0.809, 0.002, 0.336, 0.000, 0.161, 0.001, 0.104, 0.001, 0.080\}. \quad (27)$$

The first harmonic in x -polarization vanishes, the third and fifth harmonics have $f_{x;3} \simeq 0.24$ and $f_{x;5} \simeq 0.18$ [see (26)]; this is somewhat less than the respective values for $d = 0.25$: $f_{x;3} \simeq 0.28$ and $f_{x;5} \simeq 0.22$ in (23). In y -polarization [see (27)] we have $f_{y;1} \simeq 0.81 > f_{y;3} \simeq 0.34 > f_{y;5} \simeq 0.16$ for the third and fifth harmonics; note also that the ratio $f_{y;1} : f_{y;3} : f_{y;5}$ is similar to that of a common planar undulator.

Let us now consider $h = 1$, $l = 3$, $d_1 = 1$, $d_2 = 0.3$ in (21), *i.e.* the undulator field

$$\mathbf{H} = H_0[\sin(k_\lambda z), \sin(k_\lambda z) + 0.3 \cos(3k_\lambda z), 0] \quad (28)$$

[compare with equation (22)]. We obtain the following Bessel coefficients,

$$f_{x;n=1,\dots,9} = \{0.725, 0.010, 0.376, 0.012, 0.269, 0.013, 0.209, 0.013, 0.169\}, \quad (29)$$

$$f_{y;n=1,\dots,9} = \{0.725, 0.006, 0.371, 0.009, 0.262, 0.010, 0.202, 0.011, 0.162\}. \quad (30)$$

The respective numbers for each n in (29), (30) are similar for both polarizations $f_{x;n} \simeq f_{y;n}$, and the fundamental is the strongest harmonic. The spectrum in both polarizations is similar to that of a common planar undulator and does not represent particular interest.

Finally, let us consider $h = 3$, $d_1 = 0.25$, $d_2 = +1$, $l = 1$ in (21), *i.e.* the undulator field

$$\mathbf{H} = H_0[\sin(k_\lambda z), \cos(k_\lambda z) + 0.25 \sin(3k_\lambda z), 0] \quad (31)$$

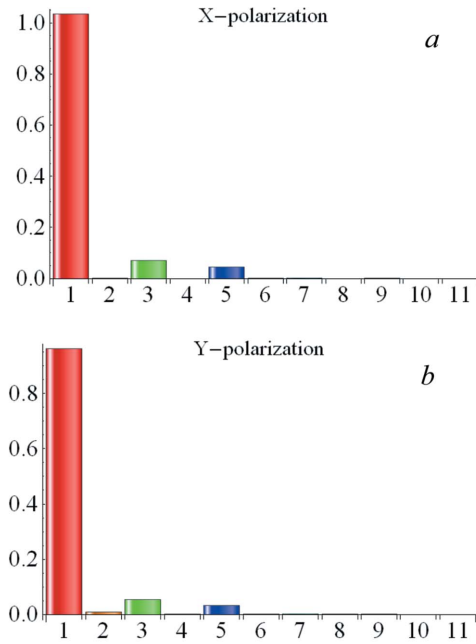


Figure 10 On-axis spontaneous UR harmonics intensity (in relative units) for the elliptic undulator with $k = 2.21622$, $h = 3$, $d_1 = +0.25$, $d_2 = 1$, $l = 1$, $\sigma_e = 10^{-4}$, $N = 30$; x -polarization (a); y -polarization (b).

[compare with (22) and (28)]. In contrast with the results for (22) in Fig. 9, we obtain for the radiation in the field (31) practically the spectrum of a helical undulator with very weak harmonic content, which does not represent particular interest (see Fig. 10); we omit proper Bessel coefficients for brevity.

5. Enhanced harmonic radiation by the phase shifting

Electrons in the magnetic field (21) with $h = 3$, $l = 1$, $d_1 = 1$, $d_2 = 0.2-0.4$ can generate intense FEL harmonics since the values of the Bessel coefficients for the first, third, fifth harmonics in x -polarization for the undulator field (22) are close to each other: $f_{y;1} \simeq f_{y;3} \simeq f_{y;5}$ [see (23)]. A simulation of FEL radiation from the undulator like (22) was proposed by Kalitenko & Zhukovskii (2020), where it was shown that elliptic bi-harmonic undulators could be potentially useful for generating powerful harmonics of the polarized FEL radiation. The enhancement of high harmonic radiation and the suppression of the fundamental tone in x -polarization are due to the field structure of the proposed undulator, but it may be difficult to build such an undulator. Evaluation of the costs of realization of this undulator in comparison with the costs of the alternative solutions, such as phase shifters between undulator segments, is beyond the scope of this paper. However, a FEL with high harmonic generation can benefit from the use of the proposed undulator with the field (21) together with the phase shifting, as we will show in the following.

It was demonstrated (McNeil *et al.*, 2006; Schneidmiller & Yurkov, 2012) that the growth of the fundamental tone power in a FEL can be reduced by the phase shift $k\pi/n$ introduced between the undulator cascades, such that $k = 2, 4, 6, \dots$ and n is the desired harmonic to be enhanced at the end. This

Table 1

Some data for the phase-shifted SASE-FEL with the undulator field (21).

Beam parameters	Relativistic factor $\gamma = 8400$, beam power $P_E = 4.3$ TW, current $I_0 = 1$ kA, current density $J = 1.573 \times 10^{11}$ A m $^{-2}$, beam section $\Sigma_{\text{beam}} = 2\pi\epsilon\beta = 6.36 \times 10^{-9}$ m 2 , average beam radius $r = (\Sigma_{\text{beam}}/\pi)^{1/2} = 45$ μm , emittances $\epsilon_{x,y}^n = \gamma\epsilon_{x,y} = 0.56$ mm mrad, $\beta = 15$ m, beam size $\sigma_{x,y} = (\epsilon\beta)^{1/2} \simeq 30$ μm , divergence $\theta = (\epsilon/\beta)^{1/2} \simeq 2$ μrad , energy spread $\sigma_e = 10^{-4}$		
Undulator parameters	$k = 3.5$, $h = 3$, $l = 1$, $d_1 = 1$, $d_2 = +0.4$, $\lambda_u = 2.8$ cm		
FEL properties:	Pierce parameter $\tilde{\rho}_n \simeq 7-9 \times 10^{-4}$, saturated lengths for the third harmonic with phase shift $L_{s3;x} \simeq 33$ m, $L_{s3;y} \simeq 28$ m, gain lengths for third harmonic $L_{\text{gain}3;x} = 1.9$ m, $L_{\text{gain}3;y} = 1.6$ m, radiation beam size $\sigma_{\text{photon}} \simeq [\sigma_{x,y}(\lambda_1 L_g/4\pi)^{1/2}]^{1/2} \simeq 20$ μm		
Harmonic number	$n = 1$	$n = 3$	$n = 5$
Bessel coefficient, f_{nx}	0.47	0.33	0.26
Bessel coefficient, f_{ny}	0.77	0.43	0.24
Pierce parameter, ρ_{nx}	0.0006	0.0005	0.0005
Pierce parameter, ρ_{ny}	0.0009	0.0007	0.0004
Harmonic wavelength, λ_n (nm)	1.75	0.58	0.35
Saturated power with phase shifts, $P_{F,n}$ (W)	3×10^9	7×10^9	7×10^6
Saturated power, no phase shifts, $P_{F,n}$ (W)	9×10^9	2×10^8	1.5×10^7

happens because the electrons obtain the spatial phase shift $k\pi/n$ between the cascades, which in fact displaces them with respect to the photon pulse; the electron microbunching at the wavelength of the fundamental tone is disrupted and the radiation power follows it. This, however, does not regard the harmonic n and its subharmonics, since the spatial phase shift $k\pi/n$, where $k = 2, 4, 6, \dots$ does not affect bunching at λ_n and its radiation. Modeling of such a FEL with a planar undulator (McNeil *et al.*, 2006; Schneidmiller & Yurkov, 2012) demonstrated that for effective harmonic suppression its bunching disruption must be repeated at every FEL gain length. Consider the cascaded FEL with the undulator and beam parameters of a LCLS ‘soft X-ray’ experiment, where the undulator field has additional periodic magnetic components (21), where $h = 3$, $l = 1$, $d_1 = 1$, $d_2 = 0.4$ (see Table 1). For the LCLS FEL planar undulator, $d_1 = d_2 = 0$ must be assumed in (21); the beam parameters remain as reported in the experiment (see Table 1).

For the bunching and FEL power modeling we use the phenomenological FEL model, based on the proposals of Dattoli & Ottaviani (2002) and Dattoli *et al.* (2004), where the saturated harmonic powers are taken accordingly accounting for the dominant third harmonic instead of the fundamental [see Zhukovsky (2018a) for planar and Zhukovsky (2019c) for elliptic undulators]. The phase shift $k\pi/3$, $k = 2, 4, 6, \dots$, aimed at enhancing the third FEL harmonic, does not affect bunching at its wavelength, but displaces electrons with respect to the radiation with wavelengths λ_1, λ_5 ; thus the harmonics with $n = 1, 5$ are rebunched repeatedly. The evolutions of the bunching and FEL power were made using *Mathematica 9* software (~ 2 s computation time on a PC),

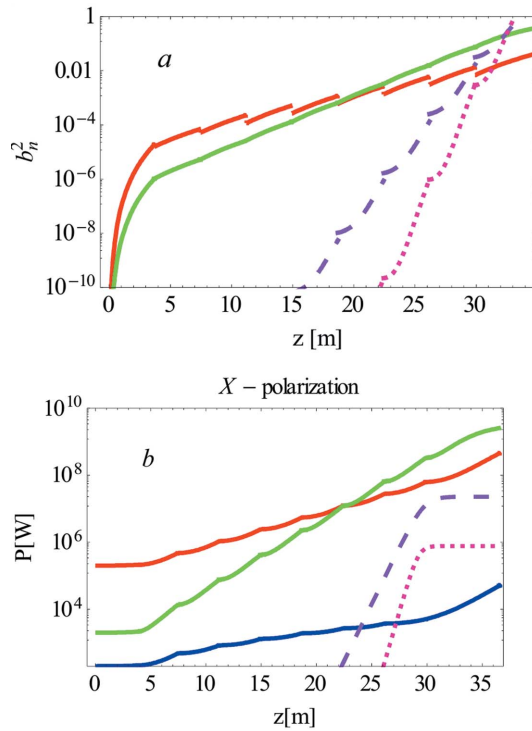


Figure 11
x-polarization: bunching coefficients (a) and FEL harmonic power (b) for the phase shifted FEL simulated for LCLS ‘low energy’ beam $E = 4.3$ GeV and undulator (21) for $h = 3, l = 1, d_1 = 1, d_2 = 0.4$. Harmonics: $n = 1$, red lines; $n = 3$, green lines; $n = 5$, blue lines. Subharmonics of the third dominant harmonic: $n = 3 \times 3$, dashed lilac line; $n = 5 \times 3$, dotted pink lines. The bunching for the weak fifth harmonic is omitted for clarity.

employing the analytical model of the FEL (Zhukovsky, 2019*a,b,c,d*) for the undulator (21), where $h = 3, l = 1, d_1 = 1, d_2 = 0.4$. The results are shown in Fig. 11 for the *x*-polarization and in Fig. 12 for the *y*-polarization. We find the following fundamental tone wavelengths and powers for the harmonics: $\lambda_1 = 1.7$ nm, $P_{\lambda=1.7\text{ nm}} = 1$ GW, and $\lambda_3 = 0.6$ nm, $P_{\lambda=0.6\text{ nm}} = 7$ GW; the fifth FEL harmonic at $\lambda_5 = 0.3$ nm is induced by the fundamental tone in *y*-polarization at the end of the FEL. Some axial asymmetry of the radiation is due to the asymmetry of the undulator field. Note that the third FEL harmonic dominates towards the end of the FEL due to the suppression of the fundamental by the phase shifting. The undulator field (21) helps by lowering the Bessel coefficient for the first and raising it for the third harmonics as compared with a planar undulator. The third FEL harmonic induces in a nonlinear regime its subharmonics at $\lambda_{3 \times 3} = 0.2$ nm and $\lambda_{3 \times 5} = 0.12$ nm. They can be weaker, because of the diffraction limit established for the approximate condition for the stable radiation: $\lambda > 4\pi\epsilon_{x,y}$. The latter inequality, though, is not strict for X-ray FELs (Pellegrini *et al.*, 2016; Huang & Kim, 2007; Saldin *et al.*, 2000; Bonifacio *et al.*, 1984; Schmüser *et al.*, 2014); high harmonics were registered even when the inequality did not hold, for example, in the LCLS experiments (Emma *et al.*, 2010; Ratner *et al.*, 2011; Emma, 2009).

Observe in Figs. 11(b) and 12(b) that the final power of the third FEL harmonic (green line) exceeds that of the funda-

mental (red line). For comparison, the LCLS FEL fundamental harmonic in the planar undulator, $d_1 = d_2 = 0$ in (21), under the same conditions was radiated with the wavelength $\lambda_1 = 1.5$ nm. The harmonic powers in the LCLS experiment with a planar undulator were as follows: $P_{\lambda_1=1.5\text{ nm}} \simeq 5$ GW, $P_{\lambda_3=0.5\text{ nm}} \simeq 70$ MW, $P_{\lambda_5=0.3\text{ nm}} \simeq 7$ MW (Emma *et al.*, 2010; Ratner *et al.*, 2011; Emma, 2009). Thus, the proposed FEL undulator field (21) for $h = 3, l = 1, d_1 = 1, d_2 = 0.4$ generated radiation at $\lambda_3 = 0.6$ nm (see Figs. 11 and 12) with the power exceeding by ~ 100 times that of the third harmonic $\lambda_3 = 0.5$ nm of the LCLS experiment under the same conditions. Moreover, subharmonics can be generated at $\lambda_{3 \times 3} = 0.2$ nm with up to ~ 30 MW power, which is several times higher than the power of the fifth LCLS harmonic at some longer wavelength $\lambda_5 = 0.3$ nm; at $\lambda_{3 \times 5} = 0.12$ nm we obtain ~ 1 MW power.

In Figs. 11(a) and 12(a) we can see that the bunching coefficients for the fundamental tone (red lines) are disrupted after every section. They grow after that until the next disruption at the next section (see Figs. 11 and 12). On the contrary, the bunching grows continuously for the third FEL harmonic (green line), as it does for the third and fifth subharmonics, denoted by the dashed lilac and dotted pink lines, respectively. The bunching for the fifth harmonic is not shown so as not to overload the figure with lines. It is disrupted as well as for the fundamental, but at lower values.

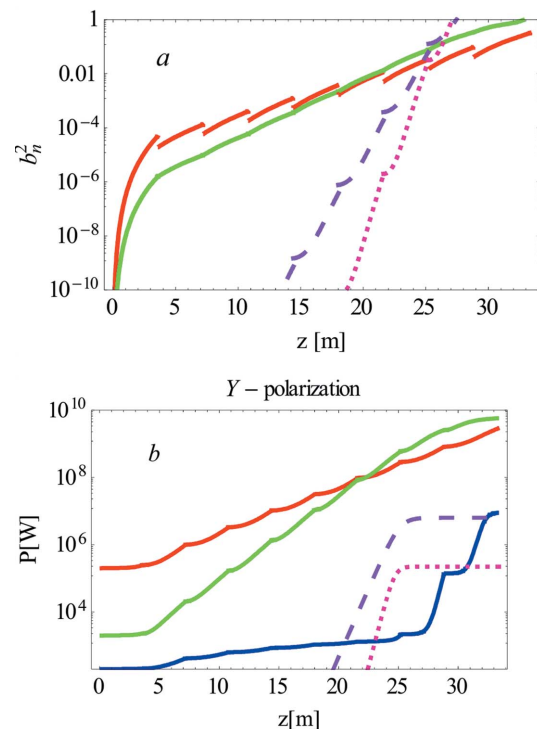


Figure 12
y-polarization: bunching coefficients (a) and FEL harmonic power (b) for the phase-shifted FEL simulated for the LCLS ‘low energy’ beam $E = 4.3$ GeV and undulator (21) for $h = 3, l = 1, d_1 = 1, d_2 = 0.4$. Harmonics: $n = 1$, red lines; $n = 3$, green lines; $n = 5$, blue lines. Subharmonics of the third dominant harmonic: $n = 3 \times 3$, dashed lilac line; $n = 5 \times 3$, dotted pink lines. The bunching for the weak fifth harmonic is omitted for clarity.

Regrouping of the electrons every time requires some distance and time; thus the continuous power growth, which follows the bunching evolution, occurs slower for the first and fifth harmonics and the third harmonics dominates at the end of the FEL.

For comparison we have modeled the evolution of the bunching and FEL power for the harmonics of the common planar undulator in the LCLS experiment for the case where the phase shifters would be installed in the same way as we supposed above under the same conditions. Despite the disruption of the bunching for the fundamental [red lines in Fig. 13(a)], this is not enough compared with the bunching for the third harmonic, and the first harmonic power [red line in Fig. 13(b)] dominates along the whole FEL. Thus, the saturation appears early due to the fundamental tone, which limits further growth of high harmonics as usual in a FEL. Eventually, the third harmonic [green line in Fig. 13(b)] does not reach the full power and its saturated power remains more than one order of magnitude lower than that of the fundamental despite the phase shifters being applied. The fifth FEL harmonic is rather strong and is shown by the blue line in Fig. 13. It grows in a nonlinear regime induced by the fundamental, and the disruption of its bunching is reflected in its power evolution in Fig. 13. This behavior of the common undulator FEL (see Fig. 13) differs from that of the asymmetric elliptic undulator FEL (see Figs. 11 and 12) where a two-period field with orthogonal polarizations helps the third UR harmonic radiation. Thus the chosen undulator with the field (21), where $h = 3$, $l = 1$, $d_1 = 1$, $d_2 = 0.4$, is much more

effective in high harmonic generation with phase shifters compared with a common planar undulator.

The above examples show possible practical solutions to increase the radiation of selected high harmonics from undulators and generate X-ray radiation from relatively low energy beams in compact installations. They demonstrate that selected high harmonics can appear in the FEL spectrum due to the third field harmonic. They also show that our phenomenological model, together with the exact formulae for the Bessel coefficients, accounting for the off-axis deviation and field harmonics, can be used for easy and fast evaluation of the FEL harmonic power, including even harmonics. This can help in controlling the deviation of the beam and the alignment of the undulator.

6. Conclusions

We have analytically considered the UR from electrons in multi-periodic undulators taking into account the field harmonics. We obtained exact analytical expressions for the UR in terms of the Bessel coefficients and UR intensities taking into account the beam properties, using the formalism of generalized Bessel functions. We have considered the general form of the two-dimensional multi-periodic magnetic field without limitations on the harmonic strength. The obtained expressions for the UR spectrum and intensity reduce in the limiting cases to those for planar and helical bi-harmonic undulators. The results are confirmed by comparison with numerical simulations and with experimental values. The analytical results are applied for FELs with the help of the phenomenological FEL model; the latter was verified with many FEL experiments and describes analytically the FEL harmonic power and bunching evolution along the undulator.

The effects of the energy spread, off-axis angle and off-axis position in the beam were analyzed and compared. Using the analytical expressions, we showed that the betatron oscillations have a negligible effect on the radiation of even UR harmonics compared with the effect of the off-axis and electron–photon interaction angles and of non-periodic magnetic components in undulators. The latter may distort the UR spectrum lines, if not screened out. An example of an LCLS undulator spectral line is demonstrated.

The shapes of the spectral lines were analytically calculated, analyzed and compared for SWISS FEL, LCLS, PAL-XFEL and LEUTL FEL taking into account the betatron split, broadening and angular effects in real beams. Theoretical radiation lines in these FELs were in agreement with data from the relevant installations and experiments. We demonstrated the betatron harmonic line split and broadening of the spectrum lines in undulators, affected by the constant field of the Earth and accounting for the off-axis effects in the finite-sized beams.

The UR radiation in a helical undulator with anti-symmetric third field harmonic was calculated using the developed analytical expressions for the Bessel coefficients. In agreement with the reported measured values, we found the second harmonic power to be $\sim 2\text{--}3\%$ of the fundamental tone. We

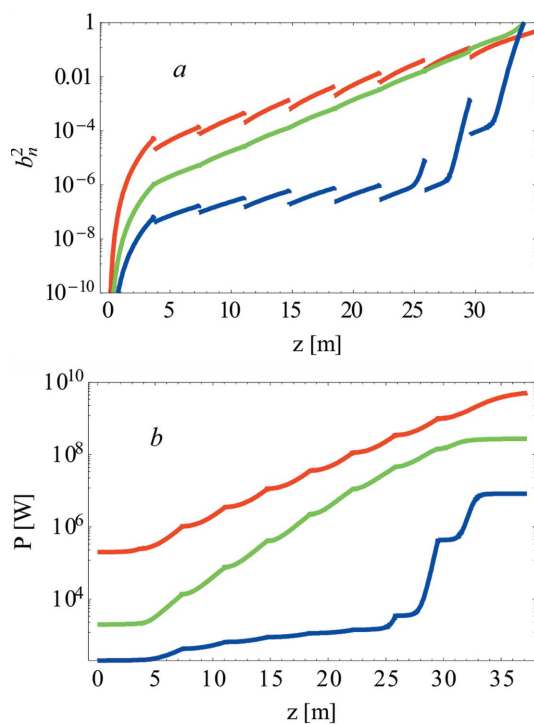


Figure 13 Evolution of the bunching coefficients (a) and FEL harmonic powers (b) for FEL harmonics in the common planar undulator FEL with phase shifters. Harmonics: $n = 1$, red lines; $n = 3$, green lines; $n = 5$, blue lines.

demonstrated that the third harmonic of the undulator field, amounting to $\sim 10\%$ strength of the main periodic field, $d \simeq 0.1$, $h = 3$, gives rise to the fifth harmonic in the UR spectrum; its radiation power is $< 2\%$ of the fundamental in agreement with the reports. A stronger third undulator field harmonic, $d \simeq 0.25$, raises the fifth UR harmonic power to $10\text{--}25\%$ of the fundamental tone, dependent on the beam quality. However, in FEL radiation the fifth harmonic remains weak due to the high sensitivity of the electron–photon interaction to the losses at high harmonic wavelengths.

We obtained exact analytical expressions for the Bessel coefficients and the UR harmonic intensity in an asymmetric elliptic bi-harmonic undulator with magnetic field (1); for the field $\mathbf{H} = H_0[\sin(k_\lambda z), d_1 \sin(hk_\lambda z) + d_2 \cos(lk_\lambda z), 0]$, we showed that strong FEL harmonics can be generated. We studied a number of combinations of the parameters h , l , d_1 , d_2 and identified the set of values $h = 3$, $l = 1$, $d_1 = 1$, $d_2 = 0.2\text{--}0.4$ which yields the values of the Bessel coefficients close to each other for the UR harmonics with $n = 1, 3, 5$; in particular, for $d_2 = 0.25$, $f_{x,n=1} = 0.29 \simeq f_{x,n=3} = 0.28 \simeq f_{x,n=5} = 0.22$. The third UR harmonic is the strongest in the y -polarization of the spontaneous radiation spectrum of this undulator, and is followed by the fundamental tone; in the x -polarization the fifth harmonic is the strongest, followed by the third, and the fundamental tone is weak.

We analytically estimated the harmonic power evolution in a single-pass FEL with this undulator. In x -polarization, the power of the third FEL harmonic reaches the power of the fundamental tone at the end of a long FEL without any phase shifters. Such an asymmetric elliptic undulator is much better for harmonic generation than a planar undulator. We demonstrated that the chosen elliptic bi-harmonic undulator could generate, in a FEL with phase shifts between the cascades, the third FEL harmonic power up to two orders of magnitude higher compared with for a planar undulator in the same FEL. This means almost 10^{10} W for 0.6 nm instead of 1.5 nm radiation for the conditions of the ‘low energy’ LCLS experiment.

Finally we note that the choice of the parameters for the beams and undulators in this study was dictated by the existing installations: KAERI (Lee *et al.*, 2015), SPARC (Giannessi *et al.*, 2011), LCLS (Emma *et al.*, 2010; Ratner *et al.*, 2011; Emma, 2009), LEUTL (Milton *et al.*, 2001), SACLA (Owada *et al.*, 2018), PAL-XFEL (Kang *et al.*, 2017) and SWISS-XFEL (Milne *et al.*, 2017; Abela *et al.*, 2017). The analysis of the harmonic generation is independent of the energies of the electron beam, although verification with experiments was made in each case for the specific values of the set of experimental parameters. The results and conclusions are valid over a broad range of electron energies from infrared to hard X-ray FELs and show the potential of elliptic bi-harmonic undulators for generating high X-ray harmonics.

References

Abela, R., Beaud, P., van Bokhoven, J. A., Chergui, M., Feurer, T., Haase, J., Ingold, G., Johnson, S. L., Knopp, G., Lemke, H., Milne,

C. J., Pedrini, B., Radi, P., Schertler, G., Standfuss, J., Staub, U. & Patthey, L. (2017). *Struct. Dyn.* **4**, 061602.
 Alexeev, V. I. & Bessonov, E. G. (1991). *Nucl. Instrum. Methods*, **A308**, 140–141.
 Bonifacio, R., Pellegrini, C. & Narducci, L. (1984). *Opt. Commun.* **50**, 373–378.
 Dattoli, G., Doria, A., Giannessi, L. & Ottaviani, P. L. (2003). *Nucl. Instrum. Methods Phys. Res. A*, **507**, 388–391.
 Dattoli, G., Giannessi, L., Ottaviani, P. L. & Ronsivalle, C. (2004). *J. Appl. Phys.* **95**, 3206–3210.
 Dattoli, G., Mikhailin, V. V., Ottaviani, P. L. & Zhukovsky, K. V. (2006). *J. Appl. Phys.* **100**, 084507.
 Dattoli, G. & Ottaviani, P. L. (2002). *Opt. Commun.* **204**, 283–297.
 Emma, P. (2009). *Proceedings of the 23rd Particle Accelerator Conference (PAC09)*, 4–8 May 2009, Vancouver, BC, Canada. TH3PBI01.
 Emma, P., Akre, R., Arthur, J., Bionta, R., Bostedt, C., Bozek, J., Brachmann, A., Bucksbaum, P., Coffee, R., Decker, F., Ding, Y., Dowell, D., Edstrom, S., Fisher, A., Frisch, J., Gilevich, S., Hastings, J., Hays, G., Hering, P., Huang, Z., Iverson, R., Loos, H., Messerschmidt, M., Miahnahri, A., Moeller, S., Nuhn, H., Pile, G., Ratner, D., Rzepiela, J., Schultz, D., Smith, T., Stefan, P., Tompkins, H., Turner, J., Welch, J., White, W., Wu, J., Yocky, G. & Galayda, J. (2010). *Nat. Photon.* **4**, 641–647.
 Giannessi, L., Alesini, D., Antici, P., Bacci, A., Bellaveglia, M., Boni, R., Boscolo, M., Briquez, F., Castellano, M., Catani, L., Chiadroni, E., Cianchi, A., Ciocci, F., Clozza, A., Couprie, M. E., Cultrera, L., Dattoli, G., Del Franco, M., Dipace, A., Di Pirro, G., Doria, A., Drago, A., Fawley, W. M., Ferrario, M., Ficcadenti, L., Filippetto, D., Frassetto, F., Freund, H. P., Fusco, V., Gallerano, G., Gallo, A., Gatti, G., Ghigo, A., Giovenale, E., Marinelli, A., Labat, M., Marchetti, B., Marcus, G., Marrelli, C., Mattioli, M., Migliorati, M., Moreno, M., Mostacci, A., Orlandi, G., Pace, E., Palumbo, L., Petralia, A., Petrarca, M., Petrillo, V., Poletto, L., Quattromini, M., Rau, J. V., Reiche, S., Ronsivalle, C., Rosenzweig, J., Rossi, A. R., Rossi Albertini, V., Sabia, E., Serafini, L., Serluca, M., Spassovsky, I., Spataro, B., Surrenti, V., Vaccarezza, C., Vecsvi, M. & Vicario, C. (2011). *Phys. Rev. ST Accel. Beams*, **14**, 060712.
 Huang, Z. & Kim, K. (2007). *Phys. Rev. ST Accel. Beams*, **10**, 034801.
 Jeevakhan, H. & Mishra, G. (2011). *Nucl. Instrum. Methods Phys. Res. A*, **656**, 101–106.
 Jia, Q. (2011). *Phys. Rev. ST Accel. Beams*, **14**, 060702.
 Kalitenko, A. M. & Zhukovskii, K. V. (2020). *J. Exp. Theor. Phys.* **130**, 327–337.
 Kang, H., Min, C., Heo, H., Kim, C., Yang, H., Kim, G., Nam, I., Baek, S. Y., Choi, H., Mun, G., Park, B. R., Suh, Y. J., Shin, D. C., Hu, J., Hong, J., Jung, S., Kim, S., Kim, K., Na, D., Park, S. S., Park, Y. J., Han, J., Jung, Y. G., Jeong, S. H., Lee, H. G., Lee, S., Lee, S., Lee, W., Oh, B., Suh, H. S., Parc, Y. W., Park, S., Kim, M. H., Jung, N., Kim, Y., Lee, M., Lee, B., Sung, C., Mok, I., Yang, J., Lee, C., Shin, H., Kim, J. H., Kim, Y., Lee, J. H., Park, S., Kim, J., Park, J., Eom, I., Rah, S., Kim, S., Nam, K. H., Park, J., Park, J., Kim, S., Kwon, S., Park, S. H., Kim, K. S., Hyun, H., Kim, S. N., Kim, S., Hwang, S., Kim, M. J., Lim, C., Yu, C., Kim, B., Kang, T., Kim, K., Kim, S., Lee, H., Lee, H., Park, K., Koo, T., Kim, D. & Ko, I. S. (2017). *Nat. Photon.* **11**, 708–713.
 Lee, K., Mun, J., Hee Park, S., Jang, K., Uk Jeong, Y. & Vinokurov, N. A. (2015). *Nucl. Instrum. Methods Phys. Res. A*, **776**, 27–33.
 Margaritondo, G. (2017). *Riv. Nuov. Cim.* **40**, 411–471.
 Margaritondo, G. & Rebernik Ribic, P. (2011). *J. Synchrotron Rad.* **18**, 101–108.
 McNeil, B. W. J., Robb, G. R. M., Poole, M. W. & Thompson, N. R. (2006). *Phys. Rev. Lett.* **96**, 084801.
 McNeil, B. W. J. & Thompson, N. R. (2010). *Nat. Photon.* **4**, 814–821.
 Milne, C., Schietinger, T., Aiba, M., Alarcon, A., Alex, J., Anghel, A., Arsov, V., Beard, C., Beaud, P., Bettoni, S., Bopp, M., Brands, H., Brönnimann, M., Brunnenkant, I., Calvi, M., Citterio, A., Craievich, P., Csatari Divall, M., Dällenbach, M., D’Amico, A.,

- Dax, A., Deng, Y., Dietrich, A., Dinapoli, R., Divall, E., Dordevic, S., Ebner, S., Erny, C., Fitze, H., Flechsig, U., Follath, R., Frei, F., Gärtner, F., Ganter, R., Garvey, T., Geng, Z., Gorgisyan, I., Gough, C., Hauff, A., Hauri, C., Hiller, N., Humar, T., Hunziker, S., Ingold, G., Ischebeck, R., Janousch, M., Juranić, P., Jurcevic, M., Kaiser, M., Kalantari, B., Kalt, R., Keil, B., Kittel, C., Knopp, G., Koprek, W., Lemke, H., Lippuner, T., Llorente Sancho, D., Löhl, F., Lopez-Cuenca, C., Märki, F., Marcellini, F., Marinkovic, G., Martiel, I., Menzel, R., Mozzanica, A., Nass, K., Orlandi, G., Ozkan Loch, C., Panepucci, E., Paraliev, M., Patterson, B., Pedrini, B., Pedrozzi, M., Pollet, P., Pradervand, C., Prat, E., Radi, P., Raguin, J., Redford, S., Rehanek, J., Réhault, J., Reiche, S., Ringele, M., Rittmann, J., Rivkin, L., Romann, A., Ruat, M., Ruder, C., Sala, L., Schebacher, L., Schilcher, T., Schlott, V., Schmidt, T., Schmitt, B., Shi, X., Stadler, M., Stingelin, L., Sturzenegger, W., Szlachetko, J., Thattil, D., Treyer, D., Trisorio, A., Tron, W., Vetter, S., Vicario, C., Voulot, D., Wang, M., Zamofing, T., Zellweger, C., Zennaro, R., Zimoch, E., Abela, R., Patthey, L. & Braun, H. (2017). *Appl. Sci.* **7**, 720.
- Milton, S. V., Gluskin, E., Arnold, N. D., Benson, C., Berg, W., Biedron, S. G., Borland, M., Chae, Y. C., Dejus, R. J., Den Hartog, P. K., Deriy, B., Erdmann, M., Eidelman, Y. I., Hahne, M. W., Huang, Z., Kim, K. J., Lewellen, J. W., Li, Y., Lumpkin, A. H., Makarov, O., Moog, E. R., Nassiri, A., Sajaev, V., Soliday, R., Tieman, B. J., Trakhtenberg, E. M., Travish, G., Vasserman, I. B., Vinokurov, N. A., Wang, X. J., Wiemerslage, G. & Yang, B. X. (2001). *Science*, **292**, 2037–2041.
- Mishra, G., Gehlot, M. & Hussain, J. K. (2009). *Nucl. Instrum. Methods Phys. Res. A*, **603**, 495–503.
- Owada, S., Togawa, K., Inagaki, T., Hara, T., Tanaka, T., Joti, Y., Koyama, T., Nakajima, K., Ohashi, H., Senba, Y., Togashi, T., Tono, K., Yamaga, M., Yumoto, H., Yabashi, M., Tanaka, H. & Ishikawa, T. (2018). *J. Synchrotron Rad.* **25**, 282–288.
- Pellegrini, C. (2016). *Phys. Scr.* **T169**, 014004.
- Pellegrini, C., Marinelli, A. & Reiche, S. (2016). *Rev. Mod. Phys.* **88**, 015006.
- Prakash, B., Huse, V., Gehlot, M., Mishra, G. & Mishra, S. (2016). *Optik*, **127**, 1639–1643.
- Ratner, D., Brachmann, A., Decker, F. J., Ding, Y., Dowell, D., Emma, P., Fisher, A., Frisch, J., Gilevich, S., Huang, Z., Hering, P., Iverson, R., Krzywinski, J., Loos, H., Messerschmidt, M., Nuhn, H. D., Smith, T., Turner, J., Welch, J., White, W. & Wu, J. (2011). *Phys. Rev. ST Accel. Beams*, **14**, 060701.
- Saldin, E. L., Schneidmiller, E. A. & Yurkov, M. V. (2000). *The Physics of Free Electron Lasers*. Springer.
- Schmüser, P., Dohlus, M., Rossbach, J. & Behrens, C. (2014). *Free-Electron Lasers in the Ultraviolet and X-ray Regime*, Vol. 258 of *Springer Tracts in Modern Physics*. Springer.
- Schneidmiller, E. A. & Yurkov, M. V. (2012). *Phys. Rev. ST Accel. Beams*, **15**, 080702.
- Tanaka, T. (2014). *Phys. Rev. ST Accel. Beams*, **17**, 060702.
- Tanaka, T. & Kitamura, H. (2001). *J. Synchrotron Rad.* **8**, 1221–1228.
- Zhukovsky, K. V. (2015a). *Moscow Univ. Phys.* **70**, 232–239.
- Zhukovsky, K. (2015b). *Opt. Commun.* **353**, 35–41.
- Zhukovsky, K. V. (2015c). *J. Electromagn. Waves Appl.* **29**, 132–142.
- Zhukovsky, K. (2016a). *Laser Part. Beams* **34**, 447.
- Zhukovsky, K. (2016b). *Nucl. Instrum. Methods Phys. Res. B*, **369**, 9–14.
- Zhukovsky, K. (2017). *J. Appl. Phys.* **122**, 233103.
- Zhukovsky, K. (2018a). *J. Opt.* **20**, 095003.
- Zhukovsky, K. V. (2018b). *Russ. Phys. J.* **60**, 1630–1637.
- Zhukovsky, K. V. (2019a). *J. Synchrotron Rad.* **26**, 1481–1488.
- Zhukovsky, K. V. (2019b). *Moscow Univ. Phys.* **74**, 308.
- Zhukovsky, K. (2019c). *Results Phys.* **13**, 102248.
- Zhukovsky, K. V. (2019d). *Moscow Univ. Phys.* **74**, 480–487.
- Zhukovsky, K. V. (2019e). *Russ. Phys. J.* **62**, 1043–1053.
- Zhukovsky, K. (2020a). *Opt. Laser Technol.* **131**, 106311.
- Zhukovsky, K. V. (2020b). *Phys. Usp.* doi: 10.3367/UFNe.2020.06.038803.
- Zhukovsky, K. (2020c). *Symmetry*, **12**, 1258.
- Zhukovsky, K. & Kalitenko, A. (2019a). *J. Synchrotron Rad.* **26**, 605–606.
- Zhukovsky, K. & Kalitenko, A. (2019b). *J. Synchrotron Rad.* **26**, 159–169.
- Zhukovsky, K. & Kalitenko, A. (2019c). *Russ. Phys. J.* **62**, 153–160.
- Zhukovsky, K. & Potapov, I. (2017). *Laser Part. Beams*, **35**, 326–336.